OPEN ACCESS
JOURNAL OF ADVANCED DIELECTRICS
Vol. 12, No. 6 (2022) 2241005 (8 pages)

DOI: 10.1142/S2010135X22410053

XI'AN JIAOTONG UNIVERSITY
World Scientific
www.worldscientific.com

Stable self-polarization in lead-free $Bi(Fe_{0.93}Mn_{0.05}Ti_{0.02})O_3$ thick films

Mengjia Fan, Xinyu Bu, Wenxuan Wang, Wei Sun, Xiujuan Lin,
Shifeng Huang and Changhong Yang*
Shandong Provincial Key Laboratory of Preparation and Measurement of Building Materials
University of Jinan, Jinan 250022, P. R. China
*mse_yangch@ujn.edu.cn

Received 21 September 2022; Revised 18 November 2022; Accepted 29 November 2022; Published 26 December 2022

The $BiFeO_3$-based film is one of the most promising candidates for lead-free piezoelectric film devices. In this work, the 1 μm-thick $Bi(Fe_{0.93}Mn_{0.05}Ti_{0.02})O_3$ (BFMT) films are grown on the ITO/glass substrate using a sol–gel method combined with spin-coating and layer-by-layer annealing technique. These films display a large saturated polarization of 95 $\mu C/cm^2$, and a remanent polarization of 70 $\mu C/cm^2$. Especially, the films are self-poled caused by an internal bias field, giving rise to asymmetric polarization-electric field (*P-E*) loops with a positive shift along the *x*-axis. A stable self-polarization state is maintained during the applied electric field increasing to 1500 kV/cm and then decreasing back. The weak dependence of *P-E* loops on frequency (1–50 kHz) and temperature (25–125°C) indicate that the internal bias field can be stable within a certain frequency and temperature range. These results demonstrate that the self-polarized BFMT thick films can be integrated into devices without any poling process, with promising applications in micro-electro-mechanical systems.

Keywords: Lead-free; stable self-polarization; bismuth ferrite; thick films.

1. Introduction

Nowadays, with the integration and miniaturization of electronic devices, it has aroused wide interest to integrate functional materials into micro-electro-mechanical systems (MEMS). Piezoelectric materials are one of the most suitable functional materials in MEMS devices. Instead of the bulk piezoelectric materials, piezoelectric films, on behalf of lead zirconate titanate (PZT) and lead magnesium niobate-lead titanate (PMN-PT), have been integrated into various devices using MEMS processes, including energy harvesters, micro-actuators and micro-sensors.[1–4]

In order to realize lead-free applications, lead-free piezoelectric films are widely studied, such as, $(Na_{0.5},Bi_{0.5})$-TiO_3-$BaTiO_3$ (NBT-BT),[5,6] $(K,Na)NbO_3$ (KNN)[7,8] and $BiFeO_3$ (BFO).[9,10] For realizing the good performance of film-based MEMS devices, the thickness of the piezoelectric film is usually greater than 1 μm.[11,12] Besides, a poling process by an external electric field is crucial prior for the films to obtain an excellent piezoelectric response, which is difficult in MEMS devices.[7,12,13] If the films are self-poled, this poling difficulty can be overcome and even the poling process can be eliminated.[5,14] Some as-deposited films with self-polarization have been discovered in recent years. The NBT-BT film can exhibit an upward self-polarization by an internal bias field, originating from the interface effect.[5] A negative build-in field of 175 kV/cm is formed in the BFO film, with a large transverse piezoelectric coefficient ($e_{31,f}$ ~ −2.8 C/m^2).[10] In addition to the greatly beneficial for device application, an enhanced photoelectric conversion efficiency has also been obtained in the self-polarization films. For example, the significant photovoltaic effect can be observed in BFO-based film, on account of that the electrons and holes could be separated by the internal electric field.[15,16]

Lead-free BFO has been investigated greatly, with a high Curie temperature of 1103 K[17,18] and a large polarization of 100 $\mu C/cm^2$,[19,20] which indicates that BFO can be a promising candidate for piezoelectric MEMS applications. However, the pure BFO films suffer a severe leakage behavior, owing to the volatilization of Bi and the valence transition of Fe ions.[21–24] Thus, only a few BFO film-based MEMS devices have been reported,[9] and the self-polarized BFO films have attracted enormous attention.[10,25] It has been reported that the oxygen vacancies can be suppressed by the introduced Mn^{2+}, thus effectively reducing the leakage current of BFO-based films.[26,27] Besides, it also acts as a sintering acid.[7] The substitution of high valance Ti^{4+} ions for the Fe site can reduce the cation valance transformation from Fe^{3+} to Fe^{2+}, which can also help to decrease the leakage current.[21] In our previous work, the strong self-polarization phenomenon was observed in the 300 nm-thick (Mn,Ti)-codoped BFO-based film deposited on flexible mica substrate.[23] A preferred upward

*Corresponding author.

polarization state was obtained with an internal bias field of 284 kV/cm under 2000 kV/cm. The film also exhibited an outstanding piezoelectric performance. Nevertheless, for better application, it is still a challenge to fabricate BFO-based films with thickness >1 μm and stable self-polarization.

In this work, we focus on the fabrication of self-polarization thick films on indium tin oxide (ITO)/glass substrate. The 1 μm-thick $Bi(Fe_{0.93}Mn_{0.05}Ti_{0.02})O_3$ (BFMT) films are prepared using a sol–gel method. The films display large saturated polarization with 95 $\mu C/cm^2$ and remanent polarization with 70 $\mu C/cm^2$. An intrinsic strong self-polarization is obtained for the BFMT thick films. Moreover, the self-polarization state is stable during the electric field increasing to 1500 kV/cm and then decreasing back, or in the frequency range of 1–50 kHz, or at working temperatures varying from 25°C to 125°C.

2. Experimental Procedure

The $Bi(Fe_{0.93}Mn_{0.05}Ti_{0.02})O_3$ thick films were grown on ITO/glass substrate using a spin-coating method followed by a layer-by-layer annealing process. To prepare the BFO-based precursor solutions, bismuth nitrate pentahydrate [$Bi(NO_3)_3 \cdot 5H_2O$], iron (III) nitrate nonahydrate [$Fe(NO_3)_3 \cdot 9H_2O$], and manganese (II) acetate tetrahydrate [$Mn(CH_3COO)_2 \cdot 4H_2O$] were dissolved together in the mixed solvents of ethylene glycol [$HOCH_2CH_2OH$] and acetic acid [CH_3COOH] with magnetic stirring at room temperature. Based on the volatility of bismuth (Bi) during thermal treatment, 5 mol.% excess Bi was added in this work. Tetrabutyl titanate [$Ti(OC_4H_9)_4$] fully dissolved in acetylacetone [$C_5H_8O_2$] was added to the solution. In order to improve the uniformity of the precursor solution and the quality of the thick films, polyethylene glycol (PEG) was added to the mixed solution. The above solution was continuously stirred for more than one day to form a transparent and stable solution. Finally, the BFMT precursor solution with a concentration of 0.5 mol/L was obtained. For the preparation of the thick films, the precursor solution was spin-coated on the ITO/glass substrate at 3000 rpm for 30 s. The spin-coated wet films were treated at 250°C for 5 min on a hot plate, and then the films were annealed at 500°C for 8 min in a rapid annealing furnace. The above spin coating and heat treatment process was repeated 15 times, and ultimately the BFMT films with a thickness of 1 μm were obtained.

The crystal structure of BFMT thick films was identified and analyzed in the 2θ range of 20–60° using an X-ray diffractometer (XRD, Bruker D8 Advance, Germany). The surface morphology and cross-sectional structure were studied by field-emission scanning electron microscope (FESEM, Zeiss Geminni300, Germany). The grain size was analyzed by Nano Measurer software. In order to conduct electrical performance test, Pt electrodes with a diameter of 200 μm were sputtered on the sample surface through a shadow mask as the top electrodes. Polarization-electric field (*P-E*) hysteresis and leakage current density-electric field (*J-E*) curves were characterized by a standard ferroelectric tester (aixACCT TF3000, Germany). The X-ray photoelectron spectroscopy (XPS) was performed by an XPS instrument (Thermo Escalab 250XI, UK). The temperature-dependent *P-E* measurements were performed by a temperature-controlled probe station (Linkam-HFS600E-PB2, UK). The capacitance was measured by an impedance analyzer (HP4294A, US).

3. Results and Discussion

As shown in Fig. 1, the typical crystal structure of BFMT thick films was revealed by the X-ray diffraction (XRD) with a 2θ ranging from 20° to 60°. The structure of the standard ITO/glass substrate was also included in the figure. Obviously, all the characteristic diffraction peaks of the BFMT thick films match well with the rhombohedral R3c structure,[28] excluding the XRD pattern of the ITO/glass substrate. Moreover, no impurity or secondary phase can be detected, demonstrating the homogeneity of the precursor solution and the suitability of the annealing process. The strong (012) and (110) diffraction peaks of the sample can be found, which is consistent with the previously reported result of pure BFO film on ITO.[29] Therefore, the well-crystallized Mn and Ti co-doping BFO-based thick films are successfully prepared on the ITO/glass substrate.

Figure 2(a) shows the surface morphology of the BFMT thick films grown on the ITO/glass substrate. It can be found that the BFMT thick films exhibit a homogeneous structure with dense and uniform nanoscale grains, suggesting that the films are well crystallized. Besides, some pinholes are scattered on the surface, which can be due to the volatilization of organic components during the layer-by-layer annealing process.[30] One-hundred randomly selected grains were analyzed

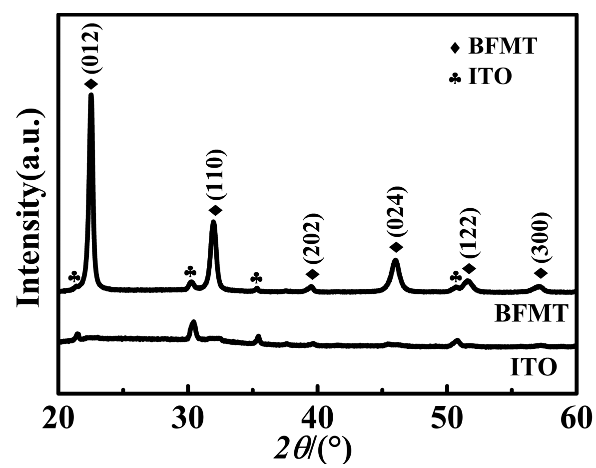

Fig. 1. XRD 2θ-scan patterns of ITO/glass substrate and BFMT thick films.

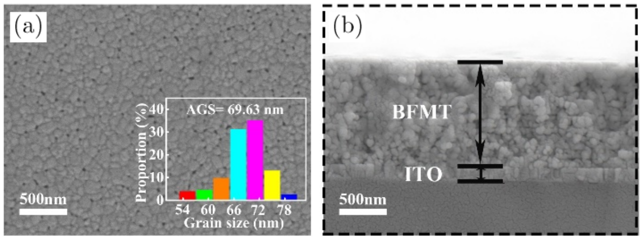

Fig. 2. (a) Surface morphology and (b) cross-sectional structure of BFMT thick films. The inset shows the relevant grain distribution.

to obtain the grain size distribution as exhibited in the inset of Fig. 2(a). The average grain size is approximately 70 nm, which is much smaller than that of pure BFO film (~120 nm).[31,32] The cross-sectional image of the BFMT/ITO/glass heterostructure is presented in Fig. 2(b). The smooth and evident film/substrate interface can be obviously observed, and the thickness is approximately 1 μm for the BFMT films.

The variation of the leakage current density (J) with the electric field (E) is illustrated in Fig. 3(a). It can be seen that the leakage current density increases with the increase of the applied electric field. In addition, the J-E curve is asymmetric under the applied positive and negative electric field, which can be caused by the asymmetry of the top (Pt) and bottom (ITO) electrodes.[33] The leakage current density measured at 300 kV/cm (~ 30 V) is ~ 3×10^{-4} A/cm^2, which is much lower than the pure BFO film (~ 1×10^{-1} A/cm^2 at 300 kV/cm).[34] For clarity, Fig. 3(b) plots the logarithmic dependence of J as a function of E. As can be seen, the J under positive bias can be divided into three regions, all of which have a slope close to 1. Meanwhile, the J under negative bias increases monotonically with a slope of 1.06. Therefore, the curves can be consistent with Ohmic conduction ($J\propto E^{\alpha}$: α~1).[35] For BFO-based films, the energy level of the oxygen vacancy is very close to the conduction band. Therefore, the electrons trapped by $V_{\ddot{O}}$ are easily activated to the conduction band by the electric field, resulting in severe leakage behavior.[21]

The XPS spectrum was carried out to analyze the valance states of Mn and Ti, as shown in Fig. 4. In Fig. 4(a), the peaks observed at the binding energy of 641.0 eV and 652.1 eV correspond to Mn^{2+} ions, while the peak located at 641.5 eV is related to Mn^{3+} ions.[36] The Ti 2p spectrum in Fig. 4(b) is

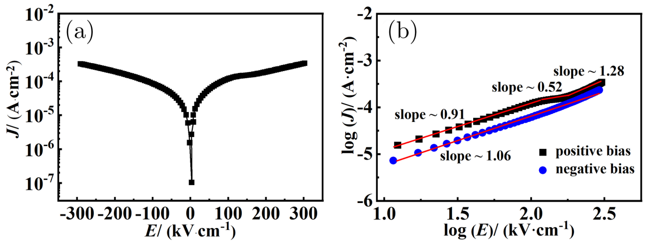

Fig. 3. (a) Leakage current density-electric field (J-E) curve of BFMT thick films; (b) log (J) versus log (E) under positive and negative biases.

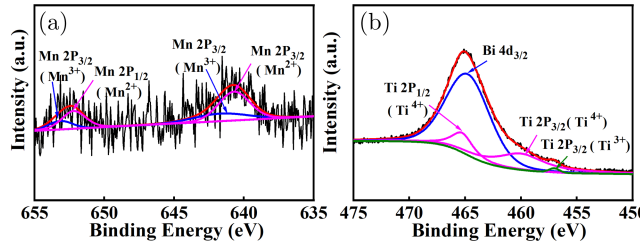

Fig. 4. XPS spectrums of (a) Mn 2p and (b) Ti 2p.

fitted with three peaks as 465.2 eV for Ti^{4+} $2p_{1/2}$, 459.4 eV for Ti^{4+} $2p_{3/2}$, 457.0 eV for Ti^{3+} $2p_{3/2}$.[37] Besides, the peak at 465.0 eV is determined to be the Bi $4d_{3/2}$ of Bi that overlaps with the Ti $2p$.[38] These results indicate that Mn^{2+} and Ti^{4+} are successfully introduced into the thick films.

In the case of the BFMT thick films, the reduced leakage current density can be attributed to the following three aspects: (i) The generation of oxygen vacancies caused by the volatilization of Bi is suppressed owing to 5 mol.% excessive Bi. (ii) The substitution of Ti ion for Fe ion can effectively inhibit the transformation from Fe^{3+} to Fe^{2+} to some extent. (iii) The $V_{\ddot{O}}$ can be reduced due to the substitution of low-valence Mn ions for Fe^{3+}. Thus, the oxygen vacancy can be decreased to a certain extent, thereby reducing the leakage current density.

The room temperature polarization-electric field (P-E) loops of BFMT thick films were measured at 10 kHz. As shown in Fig. 5(a), the typical and saturated P-E loops can be obtained for the BFMT thick films. Under the applied electric field up to 1500 kV/cm, and the values of saturated polarization (P_s) and remanent polarization (P_r) are about 95 and 70 μC/cm^2, respectively, which are much improved compared to pure BFO films.[31,32] The asymmetric P-E loops under different electric fields can be observed with a positive offset along the x-axis. Moreover, a similar asymmetry can be found in the corresponding switching current curve, as presented in Fig. 5(b). There exist two sharp current peaks in the I-V curve, which can be related to domain switching, revealing the ferroelectric nature of the BFMT thick films.[6]

Note that the coercive field (E_c) obtained from the P-E loop and I-V loop is almost the same, with asymmetry positive coercive field (E_c^+) and the negative one (E_c^-). Such asymmetry characteristic indicates that an internal bias field (E_{int}) is presented in the BFMT thick films.[39] The E_{int} can be calculated by the formula: $E_{\text{int}} = (E_c^+ + E_c^-)/2$.[16,40] Figure 5(c) exhibits the relationship between the internal bias field and the electric field. The internal bias field is up to 145 kV/cm under 500 kV/cm, suggesting the intrinsic state of the BFMT thick films with a strong self-polarization. For comparison, the P-E loops of the 12-layer and 18-layer BFMT thick films were executed under 1000 kV/cm, as shown in the inset. The E_{int} of 12-layer BFMT films is 130 kV/cm with a large E_c, and the E_{int} of 18-layer is 68 kV/cm. Compared with the other two films, the 15-layer BFMT films with a thickness of 1 μm

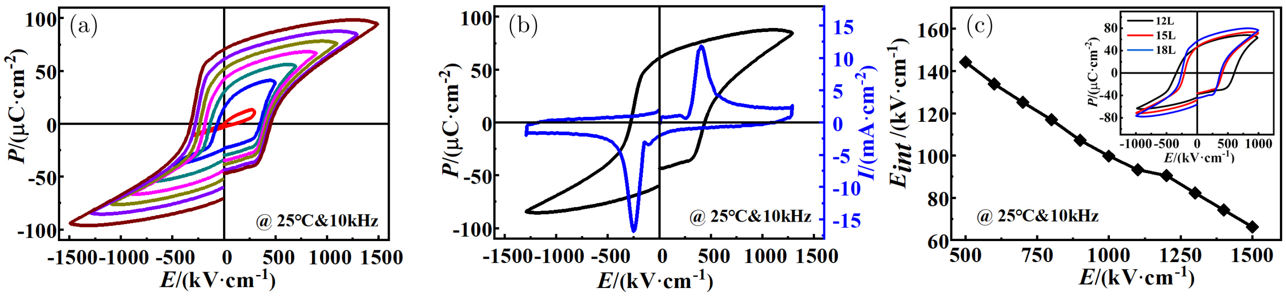

Fig. 5. (a) Room temperature *P-E* loops of BFMT thick films measured at 10 kHz. (b) *P-E* loop and corresponding switching current curve under 1300 kV/cm at 25°C and 10 kHz. (c) Internal bias field of BFMT thick films at various electric fields. The inset exhibits the *P-E* loops of BFMT thick films with 12, 15 and 18 layers under 1000 kV/cm.

Table 1. Internal bias field (E_{int}) of self-polarization films.

Films	Substrate	Synthetic method	Thickness (nm)	E_{int} (kV/cm)	Reference
PMN-PT	SRO/STO/Si	Molecular beam epitaxy	3500	−38@600 kV/cm	1
NBT-BT	Nb: STO	Sol–gel	370	19@200 kV/cm	5
BFO	FTO	Sol–gel	343	~40@100 kV/cm	16
BNFO	FTO	Chemical solution deposition	400	~150@1000 kV/cm	24
BFO	SRO/STO	Pulsed laser deposition	250	~76@240 kV/cm	41
BFMT	ITO	Sol–gel	1000	105@1000 kV/cm	This work

exhibit a large E_{int} as 105 kV/cm with a relatively small E_c. Thus, further investigations into the self-polarization of the 1 μm-thick BFMT films were carried out. Meanwhile, the E_{int} comparisons of some self-polarization films are summarized in Table 1.[1,5,16,24,41] The BFMT thick films in this work exhibit a relatively large internal bias field.

The E_{int} can originate from several possible factors: (i) The asymmetric top and bottom electrodes.[1,42] The different work functions of Pt and ITO electrodes lead to different barrier heights at the Pt/BFMT and BFMT/ITO interfaces, which can promote an internal bias field. (ii) Oxygen vacancies defect layer.[23,24] Since the deposited first film layer near the bottom electrode experiences more annealing processes, the oxygen vacancies can be accumulated at the BFMT/ITO interface, leading to the building up of an internal bias field. (iii) Defect dipoles.[43] Oriented defect dipoles, such as $(Mn_{Fe})'-(V_{\ddot{O}})$, can be formed in the BFMT thick films, generating an internal bias field and resulting in self-polarization.

To further study the self-polarization properties of the BFMT thick films, the *P-E* loops under different electric field sequences were measured, as shown in Fig. 6. The whole test process can be described as the BFMT thick films being tested from low electric fields to high electric fields, and the *P-E* loops under different electric fields are shown as the black lines in the figure. On the contrary, when the electric field comes back, the test results from the high electric field to the low electric field are displayed by red lines.

As can be seen in Fig. 6, the black curves and red curves are almost coincident. That is, the asymmetrical two curves exhibit the same positive shift under the same electric field, even experiencing from a low electric field to a high electric field and then back. This result indicates the existence of a stable self-polarization state.

In addition, it is worth noting that the asymmetry of curves becomes weaker with the increase of the electric fields, which is consistent with Fig. 5(c). As discussed above, there are three factors contributing to the internal bias field. The influence of electrodes on the weakened asymmetric characteristic can be excluded because top and bottom electrodes (Pt and ITO) are stable throughout the whole test. The electric field-induced rearrangement of oxygen vacancies can occur under high electric field,[30] which may lead to the reduction of the internal bias field. Besides, the aligned defect dipoles, which can promote self-polarization, may be broken during the high electric field measurement. The broken defect dipoles can also attribute to reduce the internal bias field.

Wide-operating frequency and high thermal stability are very important in the practical application of devices. Figure 7(a) shows the *P-E* loops of the BFMT thick films measured in the frequency range from 1 kHz to 50 kHz under 800 kV/cm at room temperature. Note that the saturated hysteresis loops can be maintained under all the test frequencies. Meanwhile, it can be found that the *P-E* loop is weakly frequency dependent, that is, the slope of dP/dE remains almost the same. The corresponding values of P_s, P_r and E_{int} at different frequencies are exhibited in Fig. 7(b). As the measuring frequency decreases from 50 to 1 kHz, the P_s and P_r values increase from 54 to 58 μC/cm^2 and

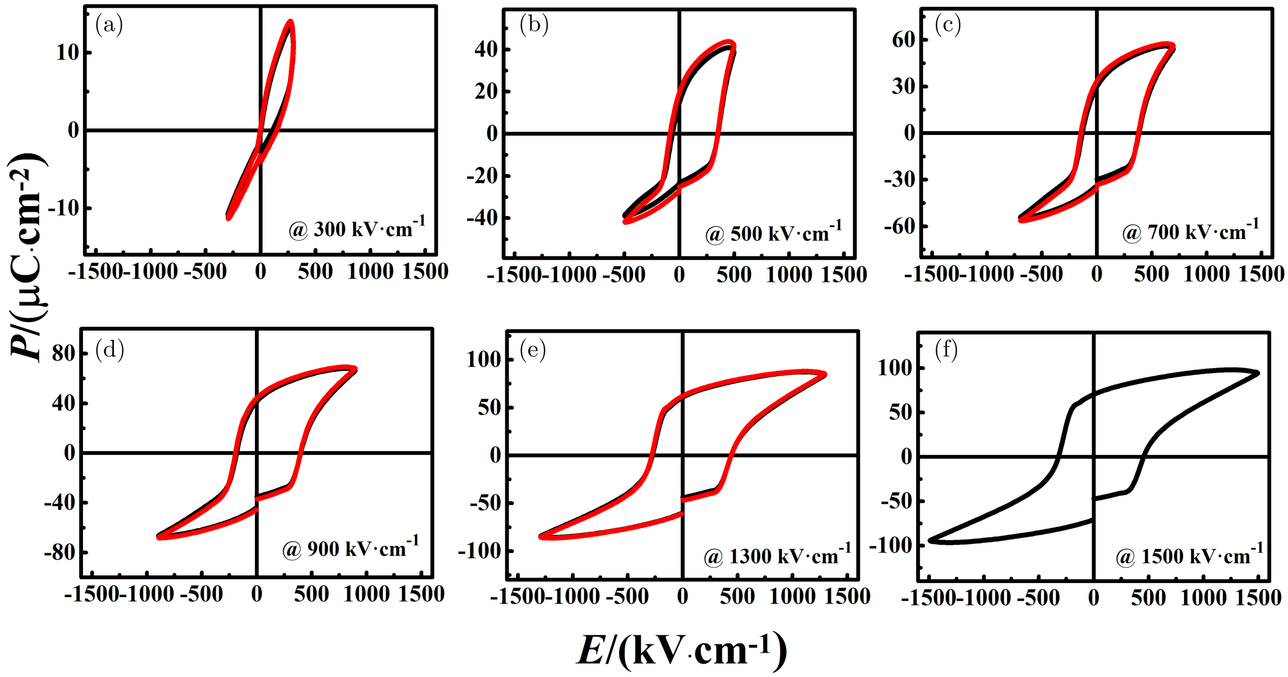

Fig. 6. (Color online) *P-E* loops under different electric fields measured during increasing and decreasing electric fields (the black loops indicate the *P-E* loops measured under the positive increasing *E* and the red loops indicate the reverse decreasing *E*).

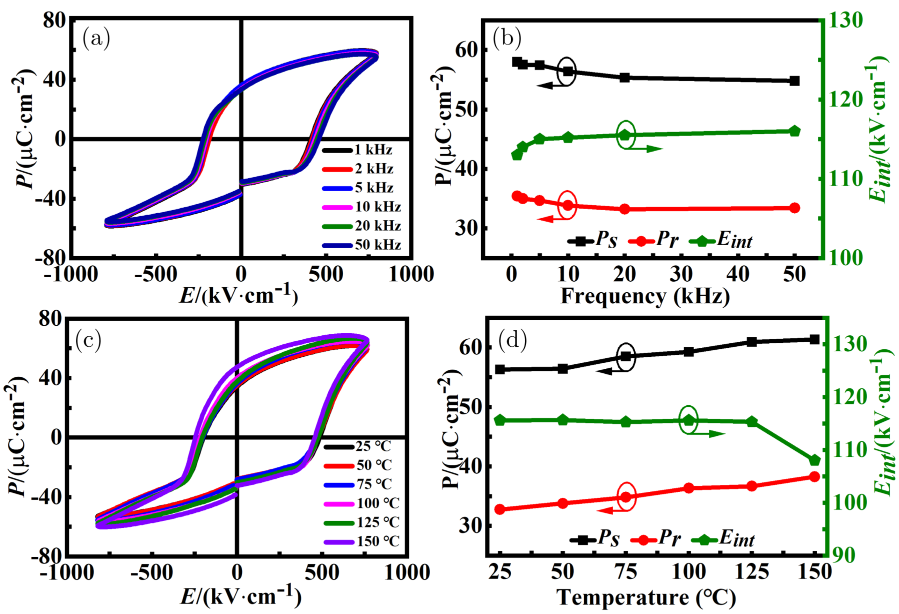

Fig. 7. (a) Frequency dependence of *P-E* loops and (b) corresponding P_s, P_r and E_{int}. (c) Temperature dependence of *P-E* loops, (d) P_s, P_r and E_{int} values as functions of temperature.

34 to 36 μC/cm^2, respectively. The E_{int} varies from 116 to 113 kV/cm, revealing that the self-polarization can remain stable in a wide frequency range. The weak dependence of *P-E* loops on frequency can be attributed to the fast switching of domains.[23] This result demonstrates the good frequency stability of the sample.

The thermal stability of the BFMT thick films was evaluated in this work by measuring under 800 kV/cm at 10 kHz in the temperature range of 25–150°C. As presented in Fig. 7(c), all the *P-E* loops exhibit typical saturated ferroelectric characteristics with a little difference under various temperature measurement environments. To clarify the temperature

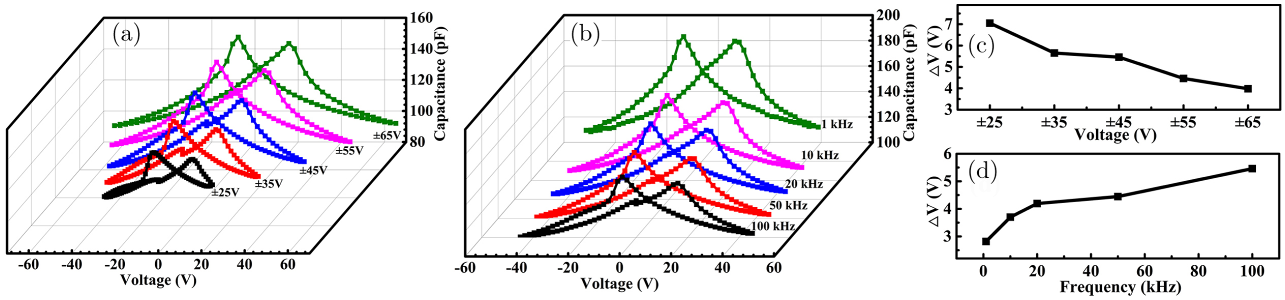

Fig. 8. (a) The *C-V* loops measured at different applied voltage. (b) The *C-V* loops measured at various frequencies under ±45V. (c,d) The corresponding Δ*V* versus applied voltage and frequency, respectively.

dependence of the sample, P_s, P_r and E_{int} as functions of temperature are depicted in Fig. 7(d). As the temperature increases from 25°C to 150°C, the values of P_s and P_r show a slight increase of 8.9% and 16.8%, respectively. This result can be contributed to the low leakage current. Similar results have been obtained in Mn and Ti co-doping BFO-based film deposited on the flexible substrate.[23] The values of E_{int} remain almost unchanged at 115 kV/cm over the temperature range of 25–125°C. However, the E_{int} drops rapidly to 108 kV/cm at 150°C, which may be related to the decoupled defect dipoles. This result demonstrates that the self-polarization of BFMT thick films can be maintained in the temperature range of 25–125°C.

The relationship between the capacitance and voltage was studied in this work to better understand the self-polarization. As presented in Fig. 8(a), the capacitance-voltage (*C-V*) loops of the BFMT thick films were measured under different direct current (DC) voltages, ranging from ±25 V to ±65 V. It is worth mentioning that the typical butterfly-shaped *C-V* loop with obvious asymmetry can be found in each curve. The asymmetric *C-V* loops shift toward the positive voltage region, which is consistent with the phenomenon observed in the *P-E* loops. Δ*V*, defined as $(|V_p|-|V_n|)/2$ (where V_p and V_n represent positive and negative switching voltage respectively), is used to characterize the degree of shift, which also originates from the existence of the internal bias in the thick films.[32,44,45] The Δ*V* gradually decreases with the increasing DC voltage, as can be seen in Fig. 8(c). At low voltages, the aligned defect dipoles maintained in the BFMT thick films can promote a self-polarization state, while these dipoles can be broken at high voltages.[32,45,46]

Figure 8(b) illustrates the frequency dependence of the *C-V* loops measured at a DC voltage of ±45 V. All the butterfly curves exhibit a right shift in the frequency range of 100–1 kHz. Corresponding Δ*V* is calculated and displayed in Fig. 8(d). As can be seen, frequency can greatly affect the value of Δ*V* of the BFMT thick films. Evidently, Δ*V* shows a reducing tendency with the decrease in measuring frequency. Similar to the phenomenon under different DC voltages, the decrease of Δ*V* is due to the reduction of internal bias. As known, the broken defect dipoles can occur due to sufficient time at a low testing frequency.[32,46,47] These results confirm that the defect dipoles can contribute to the formation of the internal bias field.

4. Conclusion

In conclusion, the 1 μm-thick BFMT films with self-polarization are deposited on ITO/glass substrate by the sol-gel technique. The BFMT is well crystallized without any detectable impurity and possesses small grain with ~70 nm. The asymmetric polarization-electric field loops and capacitance-voltage loop indicate the existence of the internal bias field. The stable self-polarization state is confirmed by the measurement under different applied electric fields, frequencies, and temperatures. The BFMT thick films with stable self-polarization are beneficial for fabricating piezoelectric MEMS devices.

Acknowledgments

This work was supported by the National Natural Science Foundation of China (Grant Nos. 51972144, U1806221 and U2006218), the Shandong Provincial Natural Science Foundation (Grant No. ZR2020KA003), the Project of "20 Items of University" of Jinan (Grant Nos. T202009 and T201907), and the Introduction Program of Senior Foreign Experts (G2021024003L), and the Shandong Provincial Key Research and Development Plan (Grant No. 2022CXPT045).

References

[1]S. H. Baek, J. Park, D. M. Kim, V. A. Aksyuk, R. R. Das, S. D. Bu, D. A. Felker, J. Lettieri, V. Vaithyanathan, S. S. N. Bharadwaja, N. Bassiri-Gharb, Y. B. Chen, H. P. Sun, C. M. Folkman, H. W. Jang, D. J. Kreft, S. K. Streiffer, R. Ramesh, X. Q. Pan, S. Trolier-McKinstry, D. G. Schlom, M. S. Rzchowski, R. H. Blick and C. B. Eom, Giant piezoelectricity on Si for hyperactive MEMS, *Science* **18**, 958 (2011).

[2]C. B. Eom and S. T. McKinstry, Thin-film piezoelectric MEMS, *MRS. Bull*. **37**, 1007 (2012).

[3]J. Jung, W. Lee, W. Kang, E. Shin, J. Ryu and H. Choi, Review of piezoelectric micromachined ultrasonic transducers and their applications, *J. Micromech. Microeng*. **27**, 113001 (2017).

[4]I. Kanno, Piezoelectric MEMS: Ferroelectric thin films for MEMS applications, *Jpn. J. Appl. Phys*. **57**, 040101 (2018).

[5]J. Y. Zhao, G. Niu, W. Ren, L. Y. Wang, G.H. Dong, N. Zhang, M. Liu and Z. G. Ye, Self-polarization in epitaxial fully matched lead-free bismuth sodium titanate based ferroelectric thin films, *ACS Appl. Mater. Interfaces* **10**, 23945 (2018).

[6]Z. Wang, J. Y. Zhao, G. Niu, W. Ren, N. Zhang, K. Zheng, Y. Quan, L. Y. Wang, J. Zhuang, H. H. Cai, X. Li, G. S. Wang, M. Liu, Z. D. Jiang and Y. L. Zhao, Giant strain responses and relaxor characteristics in lead-free $(Bi_{0.5}Na_{0.5})TiO_3$-$BaZrO_3$ ferroelectric thin films, *J. Mater. Chem. C* **10**, 7449 (2022).

[7]Y. Huang, L. Shu, F. D. Hu, L. S. Liu, Z. Zhou, Y. Y. S. Cheng, S. W. Zhang, W. Li, Q. Li, H. L. Wang, Z. N. Dong, L. Y. Wei, C. Luo and J. F Li, Implementing $(K,Na)NbO_3$-based lead-free ferroelectric films to piezoelectric micromachined ultrasonic transducers, *Nano Energy* **103**, 107761 (2022).

[8]Y. Y. S. Cheng, L. S. Liu, Y. Huang, L. Shu, Y. X. Liu, L. Y. Wei and J. F. Li, All-inorganic flexible $(K,Na)NbO_3$-based lead-free piezoelectric thin films spin-coated on metallic foils, *ACS Appl. Mater. Interfaces* **13**, 39633 (2021).

[9]M. Aramaki, T. Yoshimura, S. Murakami, K. Satoh and N. Fujimura, Demonstration of high-performance piezoelectric MEMS vibration energy harvester using $BiFeO_3$ film with improved electromechanical coupling factor, *Sens. Actuat. A-Phys*. **291**, 167 (2019).

[10]M. M. Niu, H. F. Zhu, Y. Y. Wang, J. Yan, N. Chen, P. Yan and J. Ouyang, Integration-friendly, chemically stoichiometric $BiFeO_3$ films with a piezoelectric performance challenging that of PZT, *ACS Appl. Mater. Interfaces* **12**, 33899 (2020).

[11]B. Belgacem, F. Calame and P. Muralt, Piezoelectric micromachined ultrasonic transducers with thick PZT sol gel films, *J. Electroceram*. **19**, 369 (2007).

[12]S. S Won, J. Lee, V. Venugopal, D. J. Kim, J. Lee, I. W. Kim, A. I. Kingon and S. H. Kim, Lead-free Mn-doped $(K_{0.5},Na_{0.5})NbO_3$ piezoelectric thin films for MEMS-based vibrational energy harvester applications, *Appl. Phys. Lett*. **108**, 232908 (2016).

[13]D. Shen, J. H. Park, J. H. Noh, S.Y. Choe, S. H. Kim, H. C. Wikle III and D. J. Kim, Micromachined PZT cantilever based on SOI structure for low frequency vibration energy harvesting, *Sens. Actuat. A Phys*. **154**, 103 (2009).

[14]A. V. Semchenko, V. V Sidsky, I. Bdikin, V. E. Gaishun, S. Kopyl, D. L. Kovalenko, O. Pakhomov, S. A. Khakhomov and A. L. Kholkin, Nanoscale piezoelectric properties and phase separation in pure and La-doped $BiFeO_3$ films prepared by sol-gel method, *Materials* **14**(7), 1694 (2021).

[15]H. W. Chang, F. T. Yuan, Y. C. Yu, P. C. Chen, C. R. Wang, C. S. Tu and S. U. Jen, Photovoltaic property of sputtered $BiFeO_3$ thin films, *J. Alloy. Compd*. **574**, 402 (2013).

[16]Y. J. Zhang, H. W. Zheng, X. W. Wang, H. Li, Y. H. Wu, Y. Z. Zhang, H. X. Su and G. L. Yuan, Enhanced photovoltaic properties of gradient calcium-doped $BiFeO_3$ films, *Ceram. Int*. **46**, 10083 (2020).

[17]J. Wang, J. B. Neaton, H. Zheng, V. Nagarajan, S. B. Ogale, B. Liu, D. Viehland, V. Vaithyanathan, D. G. Schlom, U. V. Waghmare, N. A. Spaldin, K. M. Rabe, M. Wuttig and R. Ramesh, Epitaxial $BiFeO_3$ multiferroic thin film heterostructures, *Science* **299**, 1719 (2003).

[18]J. C. Yang, Q. He, P. Yu and Y. H. Chu, $BiFeO_3$ thin films: A playground for exploring electric-field control of multifunctionalities, *Annu. Rev. Mater. Res*. **45**, 249 (2015).

[19]G. Catalan and J. F. Scott, Physics and applications of bismuth ferrite, *Adv. Mater*. **21**, 2463 (2009).

[20]J. G. Wu and J. Wang, $BiFeO_3$ thin films of (111)-orientation deposited on $SrRuO_3$ buffered $Pt/TiO_2/SiO_2/Si$ (100) substrates, *Acta. Mater*. **58**, 1688 (2010).

[21]G. D. Hu, S. H. Fan, C. H. Yang and W. B. Wu, Low leakage current and enhanced ferroelectric properties of Ti and Zn codoped $BiFeO_3$ thin film, *Appl. Phys. Lett*. **92**, 192905 (2008).

[22]R. Thomas, J. F. Scott, D. N. Bose and R. S. Katiyar, Multiferroic thin-film integration onto semiconductor devices, *J. Phys. Condens. Mat*. **22**, 423201 (2010).

[23]C. H. Yang, Y. J. Han, J. Qian, P. P. Lv, X. J. Lin, S. F. Huang and Z. X. Cheng, Flexible, temperature-resistant, and fatigue-free ferroelectric memory based on $Bi(Fe_{0.93}Mn_{0.05}Ti_{0.02})O_3$ thin film, *ACS Appl. Mater. Interfaces* **11**, 12647 (2019).

[24]Y. J. Han, J. Qian, J. R. Wang, X. J. Lin, C. H. Yang and S. F. Huang, Structure and ferroelectric properties of $BiFeO_3$ nano-crystalline film substituted at A/B Site, *J. Chin. Ceram. Soc*. **49**, 511 (2021).

[25]J. Yan, H. F. Zhu, J. Ouyang, I. Kanno, P. Yan, Y. Y. Wang, K. Onishi and T. Nishikado, Highly (00l)-textured $BiFeO_3$ thick films integrated on stainless steel foils with an optimized piezoelectric performance, *J. Eur. Ceram. Soc*. **42**, 3454 (2022).

[26]H. Pan, Y. Zeng, Y. Shen, Y. H. Lin, J. Ma, L. L Li and C. W. Nan, $BiFeO_3$-$SrTiO_3$ thin film as a new lead-free relaxor-ferroelectric capacitor with ultrahigh energy storage performance, *J. Mater. Chem. A* **5**, 5920 (2017).

[27]C. H. Yang, P. P. Lv, J. Qian, Y. J. Han, J. Ouyang, X. J. Lin, S. F. Huang and Z. X. Cheng, Fatigue-free and bending-endurable flexible Mn-doped $Na_{0.5}Bi_{0.5}TiO_3$-$BaTiO_3$-$BiFeO_3$ film capacitor with an ultrahigh energy storage performance, *Adv. Energy Mater*. **9**, 1803949 (2019).

[28]N. Zhang, D. Chen, F. Niu, S. Wang, L. S. Qin and Y. X. Huang, Enhanced visible light photocatalytic activity of Gd doped $BiFeO_3$ nanoparticles and mechanism insight, *Sci. Rep*. **6**, 26467 (2016).

[29]X. B. Xie, S. J. Yang, F. Q. Zhang, S. H. Fan, Q. D. Che, C. J. Wang, X. D. Guo and L. P. Zhang, Effects of excess Bi on structure and electrical properties of $BiFeO_3$ thin films deposited on indium tin oxide substrate using sol-gel method, *J. Mater. Sci-Mater. Electron*. **26**, 10095 (2015).

[30]S. J. Guo, C. H. Yang, X. M. Jiang, P. P. Lv and G. D. Hu, High ferroelectric performance of $Bi_{0.9}La_{0.1}FeO_3$ thick film by optimizing preparation precursor solution, *J. Sol-Gel. Sci. Technol*. **80**, 174 (2016).

[31]G. D. Hu, X. Cheng, W. B. Wu and C. H. Yang, Effects of Gd substitution on structure and ferroelectric properties of $BiFeO_3$ thin films prepared using metal organic decomposition, *Appl. Phys. Lett*. **91**, 232909 (2007).

[32]P. P. Lv, C. H. Yang, F. J. Geng, C. Feng, X. M. Jiang and G. D. Hu, Microstructure, ferroelectric and dielectric properties in Nd and Ti co-doped $BiFeO_3$ thin film, *J. Sol-Gel. Sci. Technol*. **78**, 559 (2016).

[33]L. X. Chen, C. Xu, X. L. Fan, X. H. Cao, K. Ji and C. H. Yang, Study on leakage current, ferroelectric and dielectric properties of BFMO thin films with different bismuth contents, *J. Mater. Sci. Mater. Electron*. **30**, 7704 (2019).

[34]Z. Y. Zhong and H. Ishiwara, Variation of leakage current mechanisms by ion substitution in $BiFeO_3$ thin films, *Appl. Phys. Lett*. **95**, 112902 (2009).

[35]P. P. Lv, X. M. Jiang, J. Yan and G. D. Hu, Stable self-polarization in Nd and Ti codoped $BiFeO_3$ films, *J. Mater. Sci-Mater. Electron*. **28**, 2233 (2017).

[36]Y. Q. Guo, P. Xiao, R. Wen, Y. Wan, Q. J. Zheng, D. L. Shi, K. H. Lam, M. L. Liu and D. Lin, Critical roles of Mn-ions in enhancing theinsulation, piezoelectricity and multiferroicity of $BiFeO_3$-based lead-free high temperature ceramics, *J. Mater. Chem. C* **3**, 5811 (2015).

[37]B. Bharti, S. Kumar, H. N. Lee and R. Kumar, Formation of oxygen vacancies and Ti^{3+} state in TiO_2 thin film and enhanced optical properties by air plasma treatment, *Sci. Rep*. **6**, 32355 (2016).

[38]N. N. Rong, M. S. Chu, Y. L. Tang, C. Zhang, X. Cui, H. C. He, Y. H. Zhang and P. Xiao, Improved photoelectrocatalytic properties of Ti-doped $BiFeO_3$ films for water oxidation, *J. Mater. Sci*. **51**, 5712 (2016).

[39]J. Lee, R. Ramesh, V. G. Keramidas, W. L. Warren, G. E. Pike and J. T. Evans, Jr. Imprint and oxygen deficiency in $(Pb,La)(Zr,Ti)O_3$ thin film capacitors with LaSrCoO electrodes, *Appl. Phys. Lett*. **66**, 1337 (1995).
[40]J. G. Chen, G. X. Jin, C. M. Wang and J. R. Cheng, Reduced dielectric loss and strain hysteresis in Fe and Mn comodified high-temperature $BiScO_3$–$PbTiO_3$ ceramics, *J. Am. Ceram. Soc*. **97**, 3890 (2014).
[41]B. C. Jeon, D. Lee, M. H. Lee, S. M. Yang, S. C. Chae, T. K. Song, S. D. Bu, J. S. Chung, J. G. Yoon and T. W. Noh, Flexoelectric effect in the reversal of self-polarization and associated changes in the electronic functional properties of $BiFeO_3$ thin films, *Adv. Mater*. **25**, 5643 (2013).
[42]Y. Liu, Y. J. Qi, P. Zhou, C. X. Guan, H. Chen, J. Z. Wang, Z. J. Ma, T. J. Zhang and Y. Liu, Mechanisms of resistive switching in $BiFeO_3$ thin films modulated by bottom electrode, *J. Phys. D. Appl. Phys*. **51**, 025303 (2018).
[43]Y. F. Hou, T. D. Zhang, W. L. Li, W. P. Cao, Y. Yu, D. Xu, W. Wang, X. L. Liu and W. D. Fei, Self-polarization induced by lattice mismatch and defect dipole alignment in (001) $BaTiO_3$/$LaNiO_3$ polycrystalline film prepared by magnetron sputtering at low temperature, *RSC Adv*. **5**, 61821 (2015).
[44]A. Z. Simões, M. A. Ramírez, C. S. Riccardi, E. Longo and J. A. Varela, Effect of oxidizing atmosphere on the electrical properties of $SrBi_4Ti_4O_{15}$ thin films obtained by the polymeric precursor method, *Solid. State. Sci*. **10**, 1951 (2008).
[45]C. Gao, J. Yang, X. J. Meng, T. Lin, J. H. Ma, J. L. Sun and J. H. Chu, Aging-induced abnormality of dielectric response under dc bias in $Ba(Zr,Ti)O_3$ thin films, *Appl. Phys. A* **104**, 123 (2011).
[46]C. H. Yang, J. Qian, Y. J. Han, J. H. Song, Q. Yao, L. X. Chen and Z. Y. Sun, The microstructure, ferroelectric and dielectric properties of Ni-doped $Na_{0.5}Bi_{0.5}TiO_3$ nanocrystalline films: A-site nonstoichiometry study, *Ceram. Int*. **44**, 5807 (2018).
[47]J. G. Wu, D. Q. Xiao, Y. Y. Wang, J. G. Zhu, J. L. Zhu and R. S. Xie, High tunability of highly (100)-oriented lead zirconate titanium thin films, *J. Am. Ceram. Soc*. **91**, 3786 (2008).